Fast-response liquid crystal lens for 3D displays

Yifan Liu,[a] Hongwen Ren,[b] Su Xu,[a] Yan Li,[a] Shin-Tson Wu[a]
[a]CREOL, The College of Optics and Photonics, University of Central Florida, Orlando, FL 32816, USA
[b]Department of Polymer Nano-Science and Engineering, Chonbuk National University, Jeonju, Jeonbuk 561-756, South Korea

ABSTRACT

Three-dimensional (3D) display has become an increasingly important technology trend for information display applications. Dozens of different 3D display solutions have been proposed. The autostereoscopic 3D display based on lenticular microlens array is a promising approach, and fast-switching microlens array enables this system to display both 3D and conventional 2D images. Here we report two different fast-response microlens array designs. The first one is a blue phase liquid crystal lens driven by the Pedot: PSS resistive film electrodes. This BPLC lens exhibits several attractive features, such as polarization insensitivity, fast response time, simple driving scheme, and relatively low driving voltage, as compared to other BPLC lens designs. The second lens design has a double-layered structure. The first layer is a polarization dependent polymer microlens array, and the second layer is a thin twisted-nematic (TN) liquid crystal cell. When the TN cell is switched on/off, the traversing light through the polymeric lens array is either focused or defocused, so that 2D/3D images are displayed correspondingly. This lens design has low driving voltage, fast response time, and simple driving scheme. Simulation and experiment demonstrate that the performance of both switchable lenses meet the requirement of 3D display system design.

Keywords: 3D, liquid crystal, microlens array, blue phase, fast response, resistive film, polymer microlens

1. INTRODUCTION

Autostereoscopic three-dimensional (3D) display is commonly recognized as an important trend for next-generation display applications in the near future.[1] Several autostereoscopic 3D display approaches have been proposed and demonstrated, such as volumetric display,[2, 3] holographic display,[4] parallax barrier display,[5, 6] and lenticular lens based display.[7-11] Among these potential solutions, the lenticular lens based design is considered as a promising candidate, due to its high optical efficiency and compatibility with current 2D display technology. The fast-response microlens array also enables 2D/3D switchability, which is highly desirable before 3D broadcast becomes commodity.

In this manuscript, we report two different fast-response cylindrical microlens array designs. The first one is a blue phase liquid crystal (BPLC) adaptive lens array driven by Pedot: PSS resistive film electrodes.[12] It not only has the advantages of other BPLC adaptive lens designs,[13-15] such as submillisecond response time and polarization insensitivity, but also exhibits other attractive features, such as relatively low driving voltage and simple driving scheme. The second lens design has a double-layered structure, including one polymeric lens layer and one twisted-nematic (TN) liquid crystal cell serving as polarization rotator.[16] The focusing power of the polymeric lens is polarization dependent. The TN cell determines the polarization direction of the incident light into the polymer lens. Therefore, by switching on/off the TN cell, the light passing through the polymer lens layer will be focused or defocused. And in turn, the 3D/2D images are displayed on the screen. The structures of these two lens designs, driving schemes, and pros and cons will be discussed in the following sections.

2. BPLC LENS DRIVEN BY PEDOT: PSS FILM ELECTRODES

2.1 Theoretical analysis

Several different BPLC adaptive microlens designs have been proposed in the past few years. One of them uses multiple stripe electrodes driven by individual voltage signals.[15] This design guarantees high quality parabolic lens profile, but the driving scheme is quite complicated. Another lens design is based on hole-patterned electrode.[13] It has a simple structure,

Advances in Display Technologies IV, edited by Liang-Chy Chien, Sin-Doo Lee, Ming Hsien Wu, Proc. of SPIE Vol. 9005, 900503 ·
CCC code: 0277-786X/14/$18 · doi: 10.1117/12.2044409

but the phase delay profile is not very good. The third BPLC lens design involves a curved top electrode, which is difficult to fabricate.[14] Besides, for all the three kinds of BPLC lenses aforementioned a dielectric layer has to be coated on the electrodes to avoid polarization sensitivity. But this extra dielectric layer shields the electric field and increases the driving voltage.[13-15]

Our BPLC lens design based on Pedot:PSS film electrodes provides an alternative solution to avoid all the problems described above. The structure of this BPLC cylindrical lens is depicted in Fig. 1.

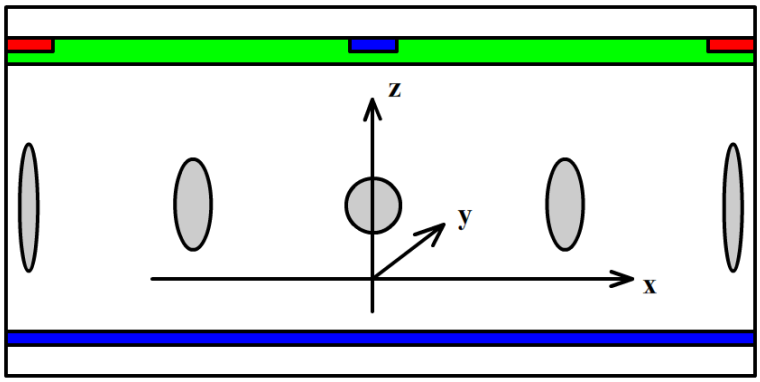

Figure 1. BPLC adaptive lens based on Pedot: PSS film electrodes.

In Fig. 1, the bottom planar electrode and top central electrode (blue) are grounded. The top edge electrodes (red) are driven by the signal voltage. The green layer coated on the top electrodes represents a resistive Pedot: PSS film, which generates gradient voltage distribution between central and edge electrodes. The gray ellipses represent the refractive index distribution of BPLC sandwiched between top and bottom substrates. As the top central electrode is grounded, the vertical electric field in the center is quite weak, and the BPLC in this region remains optically isotropic. The top edge electrodes are driven by a high voltage, so the vertical electric field is established inside the cell, which generates a large induced birefringence in the BPLC layer near the edge. Therefore, when the light passes through this cell it will experience the ordinary refractive index distribution of the BPLC layer, and the phase delay through the cell is smaller near the edge and larger in the center.

Next, we analyze the phase delay profile of this BPLC lens quantitatively. The differential equation describing the voltage distribution on the resistive film is shown as:[17, 18]

$$\nabla^2 V = \frac{\rho_R \omega \varepsilon' j}{d_R d_{LC}} V + \frac{\rho_R \omega \varepsilon''}{d_R d_{LC}} V \tag{1}$$

Here ρ_R is the resistivity of the resistive film, d_R and d_{LC} are the thickness of the resistive film and the LC layer, respectively, ω is the frequency of the driving voltage, and ε' and ε'' are the real and imaginary parts of the LC dielectric constant, respectively. For 3D displays, the aperture size of the lens is much larger than the resistive film thickness. Besides, the electric field in z direction is dominant in this cylindrical lens. And it is also taken into consideration that the voltage on the top central electrode is 0 ($V|_{x=0}=0$). In this case, Eq. (1) has an approximate solution:

$$V = \alpha \left[\exp\left(\sqrt{c} \exp\left(\left(\frac{\pi}{4} - \frac{\theta}{2} \right) j \right) x \right) - \exp\left(-\sqrt{c} \exp\left(\left(\frac{\pi}{4} - \frac{\theta}{2} \right) j \right) x \right) \right] \tag{2}$$

Here α is a positive real constant, $c = \frac{\rho_R \omega |\varepsilon^*|}{d_R d_{LC}}$, $\varepsilon^* = \varepsilon' - \varepsilon'' j = |\varepsilon^*| \exp(-j\theta)$, and θ is the phase angle.

When $\sqrt{c}|x| << 1$, the solution of Eq. (2) can be approximated by Taylor expansion as a linear relationship:

$$|V| \approx 2\alpha \sqrt{c} |x| \tag{3}$$

For a typical Pedot: PSS material, such as poly(3,4-ethylenedioxythiophene), its ρ_R= 0.01Ωm. The dielectric constant of LC material are selected as $\varepsilon'=53\varepsilon_0$ and $\varepsilon''=3.18\varepsilon_0$, where $\varepsilon_0=8.85*10^{-12}$ F/m. The device parameters are: d_R=30nm, d_{LC}=10μm, |x|≤R=200μm, and the driving voltage frequency ω=200π rad/s. Thus, we find $\sqrt{c}|x| \approx 0.02$, which satisfies the described approximation condition. Therefore, the voltage distribution on the resistive film varies linearly with the position |x| as:

$$|V| = \frac{|x|}{R} V_0 \tag{4}$$

Here V_0 is the driving voltage on the top edge electrodes.

Thus, the gradient vertical electric field is established between top and bottom substrates, and so is the gradient distribution of induced birefringence of BPLC material. Because the electric field is in vertical direction and the incident light is also in the same direction, both lights polarized in x and y directions experience the ordinary refractive index n_o of the BPLC layer, which is calculated by Eq. (5) based on Kerr model:[19, 20]

$$n_o = n_{iso} - \Delta n_{ind}/3 = n_{iso} - \lambda K E^2/3 = n_{iso} - \lambda K \frac{x^2 V_0^2}{3R^2 d_{LC}^2} \tag{5}$$

Eq. (5) is a parabolic function with respect to the location x, so the final phase delay profile of the LC lens would also have a parabolic shape. Therefore, a good parabolic lens profile is achieved with a single, very simple driving voltage signal.

However, it is also necessary to notice that Eq. (5) is valid only when the electric field is weak. If the driving voltage is too high and the vertical electric field is too strong, the Extended Kerr model will be more precise than the Kerr model in calculating the induced birefringence of BPLC material. In this case, Δn_{ind} is determined by:[21]

$$\Delta n_{ind} = \Delta n_s \left[1 - \exp\left(-\left(\frac{E}{E_s} \right)^2 \right) \right] \tag{6}$$

Here Δn_s is the saturated induced birefringence of the BPLC material, and E_s is the saturated electric field. Eq. (6) implies that if the driving voltage is too high, the phase profile of the BPLC lens will deviate from the ideal parabolic profile.

2.2 Simulation results

We performed simulation with MATLAB to validate our lens design concept. We chose the linear distribution of voltage on the resistive film as the boundary condition of the simulation, and calculated the electric field distribution inside the BPLC cell. Afterward, we calculated the induced birefringence distribution of the BPLC using Extended Kerr model. And finally, we simulated the phase profile of the lens for incident light polarized in *x* and *y* directions, respectively.

We used JNC BPLC material JC-BP01M in our simulation. The material properties are listed as follows: E_s=4.15V/μm, and Δn_s=0.142 for λ=633nm. [22]

In the first simulation, we show the phase profiles of three similar BPLC lenses with different cell gaps. The lens aperture is 2*R=400μm, and the top central electrode and top edge electrode widths are both 5μm. The cell gaps of three BPLC lenses are 6μm, 10μm, and 20μm, respectively. All three lenses are driven at 30V. Figure 2 depicts the simulated phase profiles.

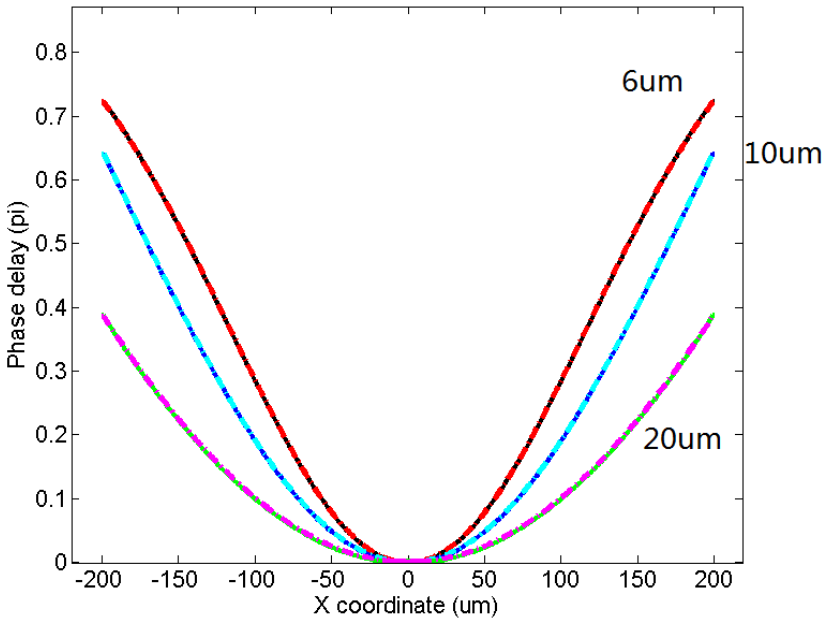

Figure 2. Simulated phase profiles of three BPLC lenses with different cell gaps. Red and black lines are for 6μm cell gap, blue and cyan lines are for 10μm, whereas green and magenta lines are for 20μm. Solid lines are phase profiles for *x* polarized light, and dash-and-dot lines are phase profiles for the *y* polarized light.

In Fig. 2, for all three cell gaps simulated the phase delay profiles overlap very well for the *x* polarized light and *y* polarized light, implying that the vertical electric field is dominant, the lateral field is negligible, and the lens is polarization insensitive. It is also noticed that as the cell gap increases, the phase delay variation from the lens edges to the lens center is decreased. This is because under the same driving voltage, a thicker cell gap results in a weaker vertical electric field, smaller induced birefringence, and longer focal length. Another observation is that in the case of 6-μm cell gap, the phase profiles are not ideal parabolic, which as we analyzed above is due to the extended Kerr effect. Thus, there is a tradeoff between minimal focal length and phase profile quality. For the device and material parameters we selected, the 10-μm cell gap seems to be an optimal choice because it provides good parabolic profile and small focal length simultaneously.

In the second simulation, we investigated the relationship between phase profile and driving voltage. Here we still use the same device and material properties as abovementioned. The cell gap is fixed at 10 μm and the driving voltages are 10V, 30V and 50V. The simulated phase delay profiles are shown in Fig. 3. For the cases of 10V and 30V, the phase profiles are still parabolic. But when the driving voltage further increases to 50V, Kerr model becomes inaccurate, and the phase profile calculated by Extended Kerr model deviates from the ideal parabolic shape.

Based on the simulated phase profile, we also fit the effective focal length of this BPLC lens. The fitting equation we used is from Refs. 14 & 15:

$$f = \frac{R^2}{2\Delta\Phi(V)} \tag{7}$$

Here *f* is the focal length, R is the half width of the lens aperture, and $\Delta\phi(V)$ is the phase delay difference between the lens edge and lens center.

Figure 4 shows the fitted focal length of the BPLC lens with respect to the driving voltage.

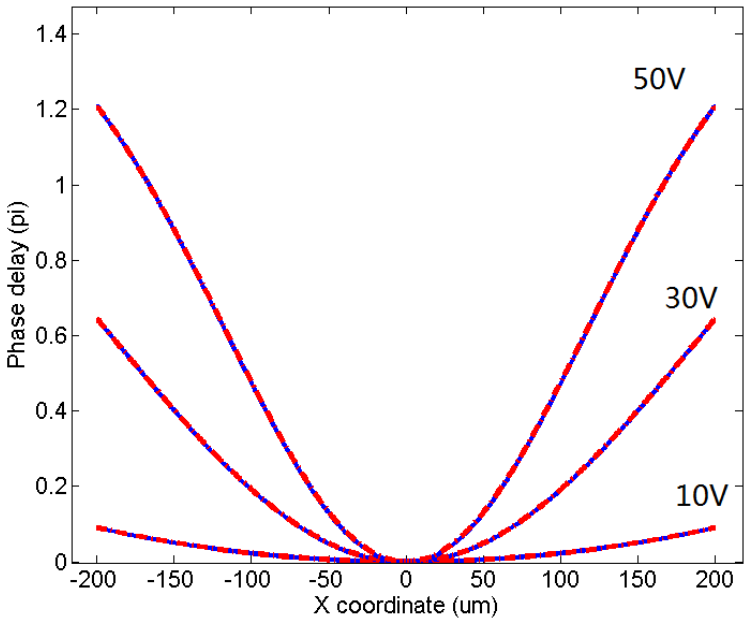

Figure 3. Simulated phase profiles of a BPLC lens under different driving voltages. Solid blue lines and dash-and-dot red lines are for *x* polarized light and *y* polarized light, respectively.

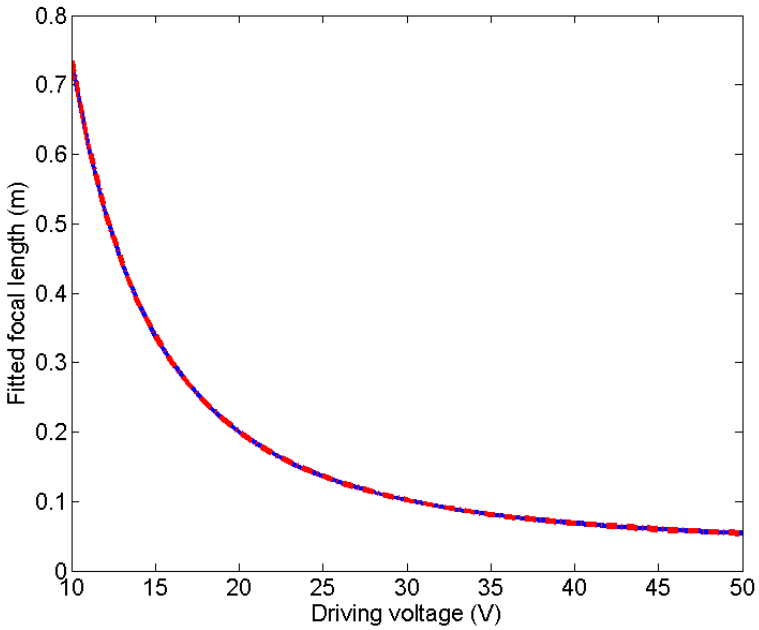

Figure 4. Simulated voltage-dependent focal length of the BPLC lens: solid blue line represents *x* polarization and dash-and-dot red lines represent *y* polarization.

In Fig. 4, when the driving voltage increases from 10V to 50V, the focal length of the lens decrease from 72cm to 6cm. This result confirms that the BPLC lens is polarization insensitive.

3. POLYMER LENS DESIGN

In the previous section, we proposed a BPLC adaptive lens based on resistive film, which exhibits several attractive features, such as submillisecond response time and polarization insensitivity. However, this lens design still suffers from some drawbacks, including high driving voltage and limited focusing power. Similar problems also exist in nematic liquid crystal lens, in which a high birefringence LC material and/or thick cell gap is required to achieve a high focusing power. But high Δn LC materials are usually associated with high viscosity or UV stability problem, whereas thick cell gap leads to high driving voltage and slow response time.[23-26] Here, we propose a polymeric lens to overcome the tradeoff between driving voltage, response time, and focusing power.[16]

3.1 Structure and operation principle

The fabrication process and device structure of the proposed polymeric lens are illustrated in Fig. 5.

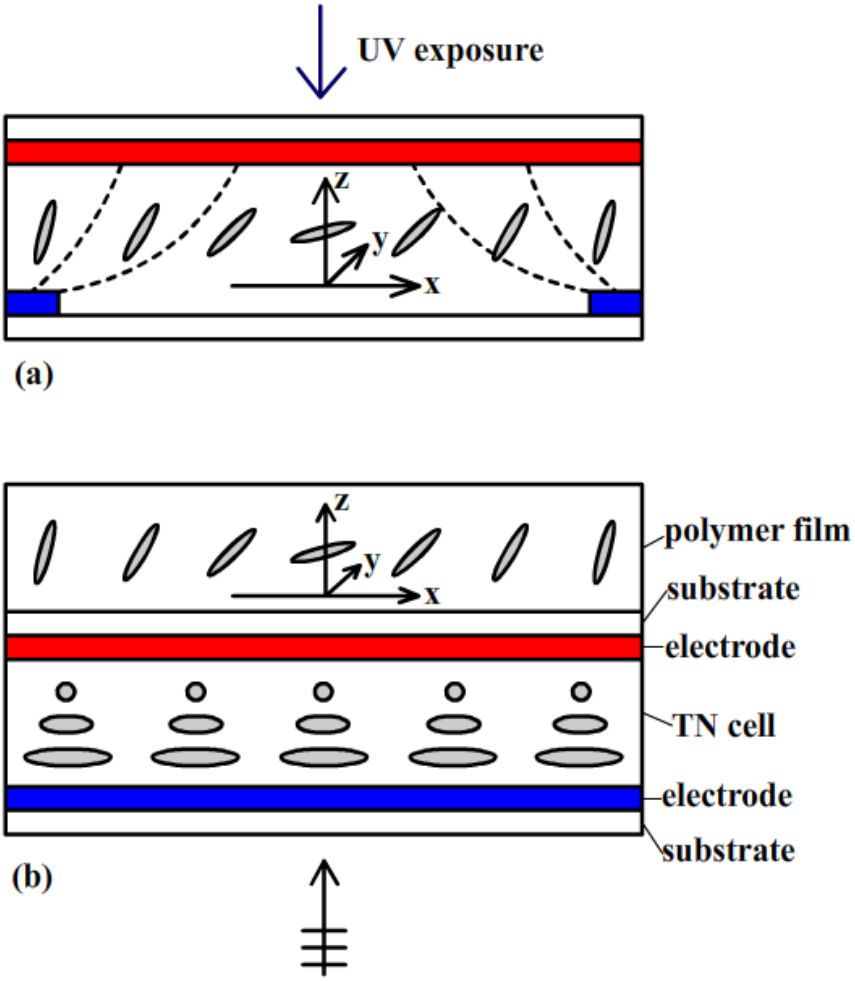

Figure 5. (a) Method for fabricating the proposed polymeric lens, and (b) structure of the polymer lens.

Fig. 5(a) shows the fabrication process of the polymeric layer whose focal length is dependent on the incident polarization. A liquid crystal monomer is filled into a homogeneous LC cell. The top electrode (red) is a planar electrode and the bottom electrodes are stripe electrodes (blue). A voltage is applied between the top and bottom electrodes so that inhomogeneous electric field establishes inside the cell, and the orientation of the LC directors becomes inhomogeneous, too. If, at this time, the light polarized in *x* direction propagates through the LC layer, it will experience a gradient refractive index (n_{eff}) distribution and get focused. But if the light polarized in *y* direction traverses the LC layer, it will

see the ordinary refractive index n_o across the LC cell, and will not be focused. To freeze the LC orientation in the voltage-on state, we could apply a UV light to polymerize the photosensitive monomer. After polymerization, the gradient refractive index distribution of the polymeric lens is fixed, so we can remove the voltage and peel off the polymeric layer from the substrates.

Fig. 5(b) shows the structure of the integrated lens, including the polymeric lens from Fig. 5(a) and a conventional TN cell. This TN cell controls the polarization direction of the incident light into the polymer lens. As depicted in Fig. 5(b), let us assume the incident light is polarized in *x* direction. When the TN cell is in its voltage-off state (V=0), the polarization direction of the light passing through the TN cell will be rotated to *y* direction, and then experiences ordinary refractive index. As a result, no focusing effect in the flat polymeric layer occurs. If the TN cell is turned on, the light through the TN cell will keep its original polarization direction, and get focused by the polymeric lens. Thus, by turning on/off the TN cell, we can switch off/on the polymeric lens and get unfocused/focused outgoing light.

The operation voltage of this polymer lens system is the V_{on} of TN cell, which can be as low as 5V. The response time of this lens is determined by the switching time of the TN cell. By using low viscosity LC material and thin cell gap, this response time can be reduced to a few milliseconds or even lower. This lens is polarization sensitive, but it is not a problem for most display applications, such as for LCD panels, because the outgoing light from the LCD screen is already linearly polarized. Comparing to other lens designs based on similar principle, our lens design use a polymer film as the light focusing layer, which is compact and light weighted[27].

3.2 Experimental results

The first step to fabricate the polymer layer is to select the proper homogeneous cells and LC monomer. In experiment, we chose a LC cell with following parameters: bottom stripe electrode width is 30μm, electrode gap is 440μm, and cell gap is 72μm. The LC monomer is a mixture of 80% BL003 LC host (Δn=0.261, n_o=1.531, $\Delta\varepsilon$=17) and 20% RM257 (n_o=1.508, n_e=1.687, $\Delta\varepsilon$=-1.5) reactive monomer. These two components were mixed and filled into the LC cell at 75°C. Then this homogeneously aligned LC cell was driven by 100Hz AC voltage and observed under polarized optical microscope. The images at λ=546nm were recorded as shown in Fig. 6.

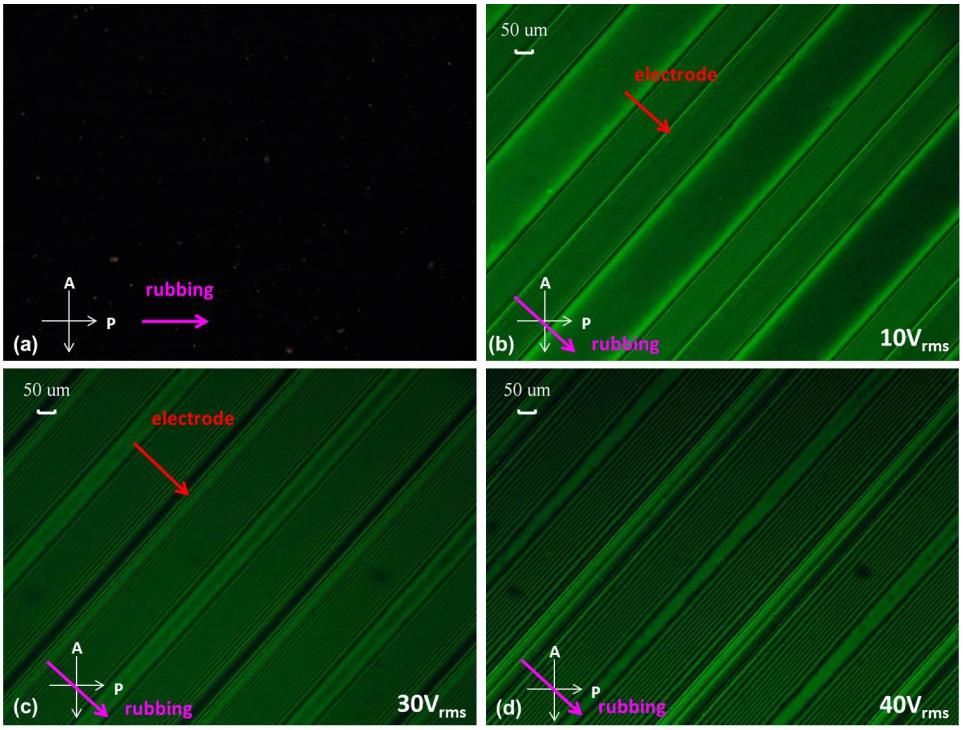

Figure 6. Images of the homogeneous LC cell: (a) Rubbing direction of the cell is parallel to the polarizer; V=0. (b) Rubbing direction of the cell is 45° to the polarizer; V=10V. (c) Rubbing direction of the cell is 45° to the polarizer; V=30V. (d) Rubbing direction of the cell is 45° to the polarizer; V=40V.

In Fig. 6(a), the analyzer and polarizer are placed in crossed state, and the alignment direction of the LC cell is parallel to the transmission axis of the polarizer. No voltage was applied to the LC cell, so the polarization direction of the traversing light was not changed and the observed image is dark. In Fig. 6(b), the LC cell was rotated by 45° in azimuthal direction, and 10V was applied. We find that fine fringes start to appear near the electrode edges, but near the aperture center there are still no fringes. This is because the electric field near the aperture center is still lower than the threshold voltage and LC molecules are not reoriented at all in this region. Then in Figs. 6(c) and 6(d), when the voltage increases to 30V and 40V, stronger electric field penetrates into the aperture center. As a result, more fringes appear near the center. As one pair of bright and dark fringes represents 2π phase retardation between the ordinary wave and extraordinary wave, we can calculate the phase delay profile of this LC lens by counting the number of fringes. It is found that under 40V driving voltage, there are 12 and a half pairs of fringes, corresponding to ~4mm focal length.

Then the LC cell was cured under 20mW/cm^2 of UV light (λ~365nm) for 5 hours. After that, the polymerized LC layer was peeled off the substrates. The film was observed under microscope again, and result is shown in Fig. 7. In Fig. 7(a) the interference fringes are similar to the image in Fig. 6(d), proving that the film is not damaged after peeling off. In Fig. 7(b) the polymer film was rotated by 45° in azimuthal direction. A good dark state is demonstrated in the electrode gap region, which is similar to Fig. 6(a). But near the electrode stripes there is some light leakage, which might be due to the disclination lines of LC molecules caused by the driving voltage. In Fig. 7(c) the analyzer was removed and the microscope was adjusted to observe the focal plane of the LC film lens. The focal spots are parallel bright stripes, each of which corresponds to one cylindrical polymeric lens. The narrow focal spot lines convince that the focusing capability of the polymeric lens is quite good. But there is still weak light leakage surrounding the focal spots, which might be due to the twisted alignment of LC molecules caused by misalignment of top and bottom substrates. Finally, in Fig. 7(d), the polarizer was rotated by 90°, so that the incident light became ordinary wave. There was no focusing effect by the polymeric layer, so the uniform, bright outgoing light was observed across the polymer film.

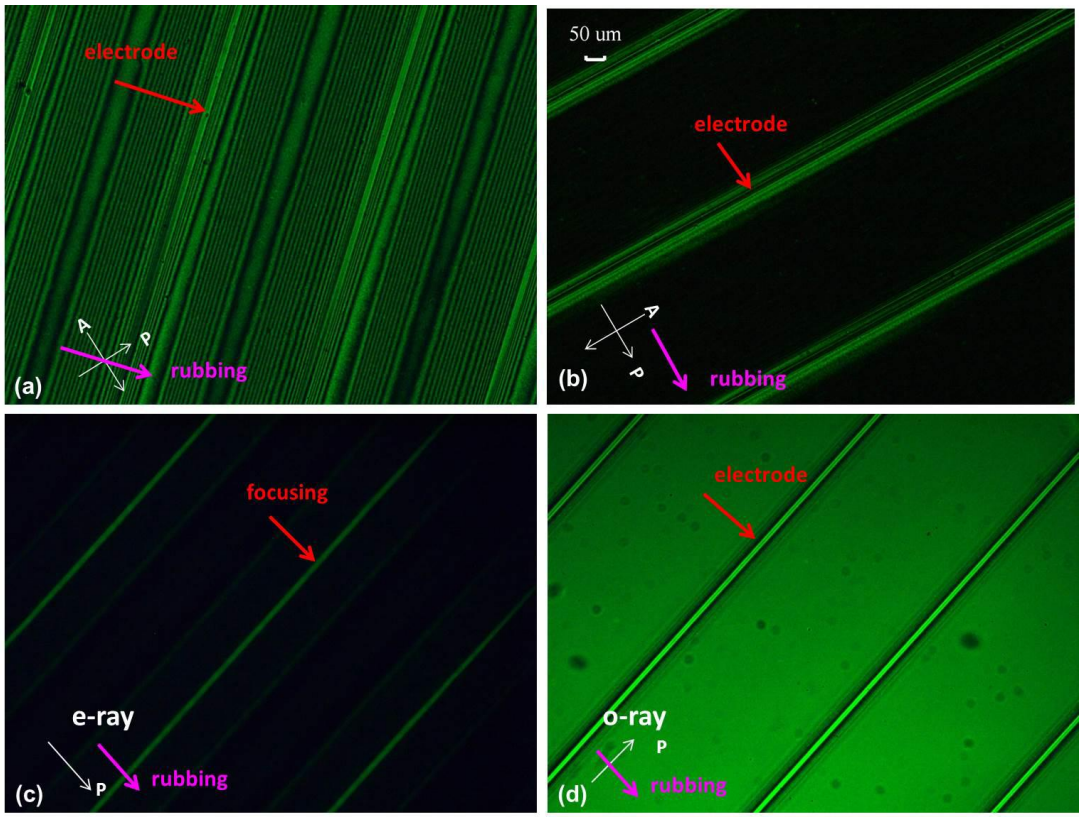

Figure 7. Images of the LC polymer film: (a) LC orientation direction of the film is 45° to the polarizer. (b) LC orientation direction of the film is parallel to the polarizer. (c) LC orientation direction of the film is parallel to the polarizer. The analyzer is removed and the focusing plane of the film is recorded. (d) LC orientation direction of the film is perpendicular to the polarizer. The analyzer is removed.

Then a TN cell was prepared as the switchable polarization rotator. The cell gap of the TN cell was 5μm, and E7 LC mixture (Δn= 0.2253; viscosity= 39cp; $\Delta\varepsilon$= 13.8) was filled into the TN cell. The polymer film was laminated to the surface of this TN cell. Testing result shows that when the TN cell is turned on and off, the lens switches between non-focusing and focusing states. The unfocused/focused light observed under microscope is similar to Fig. 7(d) and Fig. 7(c), respectively.

The response time of this lens was also tested. When the TN cell was driven by a 10V AC voltage, the rise time (from non-focusing to focusing) was ~1ms, and the decay time (from focusing to non-focusing) ~15ms. This response time is faster than that of a conventional LC lens in which a thick LC layer has to be driven directly by a fairly high voltage.[23] As mentioned before, this response time could be further improved if a better nematic LC material and optimized TN cell gap are selected.

4. CONCLUSION

We demonstrate two different LC adaptive lens designs to meet the requirement of 2D/3D switchable display applications. The first design is a blue phase liquid crystal lens based on resistive film electrode. This design exhibits submillisecond response time, polarization insensitivity, simple driving scheme and relatively low voltage as compared to other BPLC lenses. But the minimal focal length is still too long due to the limited induced birefringence of BPLC material. The second lens design is the combination of a birefringent polymeric lens and a TN cell. This lens design also possesses a fast response time, short focal length and low driving voltage.

REFERENCES

[1] Pastoor, S. and Wopking, M., "3-D displays: A review of current technologies," Display 17, 100-110 (1997).
[2] MacFarlane, D., "Volumetric three-dimensional display," Appl. Opt. 33(31), 7453-7457 (1994).
[3] Xia, X., Zheng, Z., Liu, X., Li, H. and Yan, C., "Omnidirectional-view three-dimensional display system based on cylindrical selective-diffusing screen," Appl. Opt. 49(26), 4915-4920 (2010).
[4] Yoshikawa, H. and Yamaguchi, T., "Computer-generated holograms for 3D display," Chinese Optic. Lett. 7(12), 1079-1082 (2009).
[5] Peterka, T., Kooima, R. L., Sandin, D. J., Johnson, A., Leigh, J. and DeFanti, T. A., "Advances in the dynallax solid-state dynamic parallax barrier autostereoscopic visualization display system," IEEE Tran. On Visualization and Computer Graphics 14(3), 487-499 (2008).
[6] Tao, Y., Wang, Q., Gu, J., Zhao, W. and Li, D., "Autostereoscopic three-dimensional projector based on two parallax barriers," Opt. Lett. 34(20), 3220-3222 (2009).
[7] Choi, H., Park, J.-H., Kim, J., Cho, S.-W. and Lee, B., "Wide-viewing-angle 3D/2D convertible display system using two display devices and a lens array," Opt. Expr. 13(21), 8424–8432 (2005).
[8] Dekker, T., de Zwart, S. T., Willemsen, O. H., Hiddink, M. G. H. and IJzerman, W. L., "2D/3D switchable displays," Proc. SPIE 6135, 61350K, 61350K-11 (2006).
[9] Takagi, A., Saishu, T., Kashiwagi, M., Taira, K. and Hirayama, Y., "Autostereoscopic partial 2-D/3-D switchable display using liquid-crystal gradient index lens," SID Symp. Dig. 41, 436–439 (2010).
[10] Huang, Y. P., Liao, L. Y. and Chen, C. W., "2-D/3-D switchable autostereoscopic display with multi-electrically driven liquid-crystal (MeD-LC) lenses," J. Soc. Inf. Disp. 18(9), 642–646 (2010).
[11] Liu, Y., Ren, H., Xu, S., Chen, Y., Rao, L., Ishinabe, T. and Wu, S.-T., "Adaptive focus integral image system design based on fast-response liquid crystal microlens," J. Disp. Tech. 7(12), 674–678 (2011).
[12] Li, Y., Liu, Y., Li, Q. and Wu, S.-T., "Polarization independent blue-phase liquid crystal cylindrical lens with a resistive film," Appl. Opt. 51(14), 2568-2572 (2012).
[13] Lin, Y. H., Chen, H. S., Lin, H. C., Tsou, Y. S., Hsu, H. K. and Li, W. Y., "Polarizer-free and fast response microlens arrays using polymer-stabilized blue phase liquid crystals," Appl. Phys. Lett. 96, 113505 (2010).
[14] Li, Y. and Wu, S.-T., "Polarization independent adaptive microlens with a blue-phase liquid crystal," Opt. Expr. 19(9), 8045–8050 (2011).

[15] Lee, C. T., Li, Y., Lin, H. Y. and Wu, S.-T., "Design of polarization independent multi-electrode GRIN lens with a blue-phase liquid crystal," Opt. Expr. 19(18), 17402–17407 (2011).
[16] Ren, H., Xu, S., Liu, Y. and Wu, S.-T., "Switchable focus using a polymeric lenticular microlens array and a polarization rotator," Opt. Expr. 21(7), 7916-7925 (2013).
[17] Naumov, A. F. and Vdovin, G., "Multichannel liquid-crystal based wave-front corrector with modal influence functions," Opt. Lett. 23(19), 1550–1552 (1998).
[18] Naumov, A. F., Loktev, M. Y., Guralnik, I. R. and Vdovin, G., "Liquid-crystal adaptive lenses with modal control," Opt. Lett. 23(13), 992–994 (1998).
[19] Kerr, J., "A new relation between electricity and light: dielectrified media birefringent," Philos. Mag. 50(332), 337–348 (1875).
[20] Yan, J., Li, Y. and Wu, S.-T., "High-efficiency and fast-response tunable phase grating using a blue phase liquid crystal," Opt. Lett. 36(8), 1404–1406 (2011).
[21] Yan, J., Cheng, H. C., Gauza, S., Li, Y., Jiao, M., Rao, L. and Wu, S.-T., "Extended Kerr effect of polymer-stabilized blue-phase liquid crystals," Appl. Phys. Lett. 96, 071105 (2010).
[22] Cheng, H. C., Yan, J., Ishinabe, T. and Wu, S.-T., "Vertical field switching for blue-phase liquid crystal devices," Appl. Phys. Lett. 98, 261102 (2011).
[23] Commander, L. G., Day, S. E. and Selviah, D. R., "Variable focal length microlenses," Opt. Commun. 177(1-6), 157–170 (2000).
[24] Fan, Y.-H., Ren, H., Liang, X., Wang, H. and Wu, S.-T., "Liquid crystal microlens arrays with switchable positive and negative focal lengths," J. Disp. Tech. 1(1), 151–156 (2005).
[25] Liu, Y. J., Sun, X. W. and Wang, Q., "A focus-switchable lens made of polymer–liquid crystal composite," J. Cryst. Growth 288(1), 192–194 (2006).
[26] Na, J.-H., Park, S.-C., Kim, S.-U., Choi, Y. and Lee, S.-D., "Physical mechanism for flat-to-lenticular lens conversion in homogeneous liquid crystal cell with periodically undulated electrode," Opt. Expr. 20(2), 864–869 (2012).
[27] Flack, J., Harrold, J. and Woodgate, J., "A prototype 3D mobile phone equipped with a next generation autostereoscopic display," Proc. SPIE 6490, 64900M (2007).